Korean J. Chem. Eng., 40(11), 2671-2682 (2023)
DOI: 10.1007/s11814-023-1412-4

pISSN: 0256-1115
eISSN: 1975-7220

Modeling of heterogeneous fenton process using catalyst produced from date palm waste for dye removal: Catalyst characterization and process optimization

Faeze Moslemi, Mohammad Hassan Ehrampoush, Mohammad Mehralian, and Arash Dalvand†

Environmental Science and Technology Research Center, Department of Environmental Health Engineering, School of Public Health, Shahid Sadoughi University of Medical Sciences, Yazd, Iran
(*Received 29 October 2022 • Revised 4 February 2023 • Accepted 2 March 2023*)

Abstract−This study evaluated the efficiency of the heterogeneous Fenton process using magnetic activated carbon catalyst produced from date palm waste in removing direct dye from aqueous solutions. The experimental runs and optimal conditions for the effect of contact time, solution pH, catalyst dose, and persulfate dose were determined based on the Box-Behnken design under response surface methodology (RSM). FTIR, FESEM, XRD, EDS, BET, and VSM analyses were used to investigate the characteristics of the catalyst. The analysis of variance (ANOVA) verified that the selected statistical model with R^2 0.95, p-value<0.0001, and F-value 58.67 was significant. The results of optimal conditions showed that at a dye concentration of 50 mg/L, catalyst dose 0.96 g/L, persulfate dose 9.7 mM, pH 7 and contact time 84 min, maximum removal efficiency of DR80, DB80, DBw103 and COD was 92.69, 97.07, 73.85, and 60%, respectively. After five cycles of catalyst regeneration, the results showed that the catalyst could be utilized several times effectively for dye removal.

Keywords: Box Behnken Design, Direct Dye Removal, Heterogeneous Fenton Process, Magnetic Activated Carbon Catalyst, Modeling

INTRODUCTION

Environmental pollution caused by the discharge of effluents containing organic dyes into water has become a global issue that seriously endangers human health [1]. The textile industry can be considered one of the industries in which wastewater has a significant potential for pollution [2]. About 10% of the dyes used in these industries are discharged into the environment [3]. Azo dyes are the largest group of synthetic dyes [4-6], and 70-60% of the total consumption of available dyes is related to them [7].

Azo dyes are toxic due to the presence of aromatic amine groups in their structure and have harmful effects on human health and the environment [8,9]. Most direct dyes, such as Direct Red 80 (DR80) used in the present study are azo dyes commonly used in the textile industry [10]. Azo dyes are widely used in the textile, paper, food, leather, and cosmetic industries [11,12]. Some dyes can lead to severe damage to humans such as kidney dysfunction [13], central nervous system damage [14] and prolonged contact causes damage to the respiratory system and skin allergies (dermatitis) [5,8,13] as well as Tachycardia (rapid heartbeat) and eye burns [13]. Their excretion into the hydrosphere, even at very low concentrations, disrupts photosynthesis [1] and adversely affects aquatic life [2].

Various methods for dye removal have been applied to reduce its impact on the environment, including coagulation, filtration, ion exchange, biological treatment, electrolysis, activated sludge, and solvent extraction [4,7]. Problems due to these methods are high cost, disposal of toxic by-products, lack of effective dye reduction [15], the unwanted odor of the fermentation process and production of large amounts of sludge [14], relative inefficiency and time-consuming [16]. So, textile wastewater treatment is still a major constraint.

Recently, advanced oxidation processes (AOPs) due to the production of highly potent oxidizing species ($OH^{\bullet}$, $SO_4^{\bullet}$, $O_2^{\bullet}$) and their ability to degrade highly emerging contaminants have been considered [16-19]. Fenton oxidation is a simple process of advanced catalyst-based oxidation. Compared to other AOPs, Fenton processes have a wide range of applications, simple operation, degradation and rapid mineralization [15], high performance, simplicity and non-toxicity [20].

To overcome the disadvantages of the homogeneous Fenton process, such as limited optimal pH (2-4) [21], high operating costs, production of large amounts of iron sludge [22-24] and problems in catalyst recycling [16,20], heterogeneous Fenton processes have been developed in recent years. Sreej et al. investigated homogeneous and heterogeneous photo-Fenton processes for textile wastewater treatment. The heterogeneous process showed the highest removal efficiency under the optimum conditions with COD and dye removal (62% and 85%, respectively). Also, for the homogeneous photo-Fenton process, COD and dye removal reached 47% and 82%, respectively [25].

H_2O_2 has long been utilized in Fenton systems to generate ($-OH^{\bullet}$) radicals. However, there are drawbacks to this system [18]; H_2O_2 is a costly and dangerous chemical [26], high performance in limited pH (2-4), instability of H_2O_2 during transportation and storage, and high consumption of H_2O_2 during work [18]. Sulfate-based AOPs (SR-AOPs) are increasingly being considered a suitable alter-

†To whom correspondence should be addressed.
E-mail: arash.dalvand@gmail.com

native to H_2O_2-based Fenton due to their many advantages over hydroxyl radical-based (-OH) processes. Recent studies show that sulfate radicals are more effective than hydroxyl radicals in removing dyes in the aqueous system [27].

Activated carbon is one of the options considered by researchers due to its porous structure, high specific surface area, abundance of surface functional groups and high adsorption capacity for pollutant removal [1,3,7]. However, the cost of producing activated carbon is very high. Hence, agricultural waste is known as a suitable alternative for the production of cost-effective activated carbon [3,4,7]. Agricultural waste from readily available sources such as barley husk, wheat straw, almond gum, garlic straw [4], and rice husk [16], has been successfully applied to remove dyes from aqueous solutions. Iran is the third-largest producer of dates in the world. Only 5 percent of the waste produced by date palm trees is used beneficially in Iran; the rest is burned or disposed of in the environment, which is an environmental challenge [28]. Changing date palm waste to valuable products such as activated carbon and its application for pollutants removal from the aqueous solution will reduce the related environmental problems.

One of the most important disadvantages of using activated carbon (AC) is its difficult separation and removal from the water after the experiments. The use of magnetic nanoparticles for wastewater treatment in addition to their potential to treat large amounts of wastewater in a short duration has been considered due to the easy preparation and easy separation [29], as well as the possibility of reusing the catalyst during the experiment [26].

The aim of this study was to investigate the efficiency of the heterogeneous Fenton process using magnetic activated carbon catalyst produced from date palm waste in direct dye removal from aqueous solutions, which has not been considered till now. Also, the most important operating parameters, including contact time, solution pH, catalyst dose, and persulfate dose optimized by statistical models and the interaction effect of the parameters, were investigated.

MATERIALS AND METHODS

1. Materials

Materials required in this study included phosphoric acid (H_3PO_4) with 85% purity, hydrochloric acid (HCl), potassium persulfate ($K_2S_2O_8$), ferrous sulfate ($FeSO_4{\cdot}7H_2O$), ferric chloride ($FeCl_3{\cdot}6H_2O$), sodium hydroxide (NaOH), and ethanol were from Merck Co, Germany. COD vial (150 mg/L) provided from HACH, USA. Direct Red 80 (DR80) (Table 1), Direct Blue 80 (DB80) (Table 2), and Direct Brown 103 (DB103) (Table 3) were purchased from CHT/BEZEMA Co.

Table 1. Properties of direct Red 80

Dye	C. I. Direct Red 80
Chemical structure	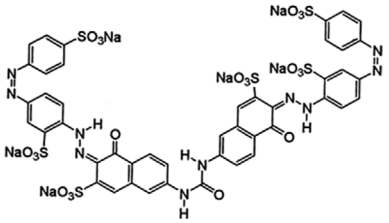
Chemical formula	$C_{45}H_{26}N_{10}Na_6O_{21}S_6$
λmax (nm)	528
Molecular weight (g/mol)	1,373.07

Table 2. Properties of direct Blue 80

Dye	C. I. Direct Blue 80
Chemical structure	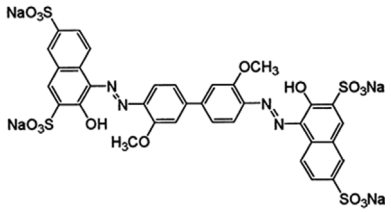
Chemical formula	$C_{32}H_{14}Cu_2N_4Na_4O_{16}S_4$
λmax (nm)	570
Molecular weight (g/mol)	1057.8

Table 3. Properties of direct brown 103

Dye	C. I. Direct Brown 103
Chemical structure	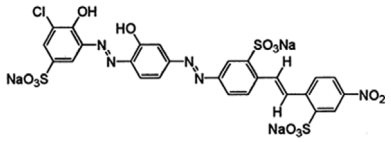
Chemical formula	$C_{26}H_{15}ClN_5Na_3O_{13}S_3$
λmax (nm)	430
Molecular weight (g/mol)	806.04

2. Synthesis of Activated Carbon from Date Palm Tree Wastes

Date palm tree fibers, after collection, were washed several times with water to remove dust and contaminants, then crushed and placed in the oven at 120 °C for 2 hours, until completely dry. Then, in a ratio of 1 : 1, concentrated phosphoric acid was added to the fibers and placed at 120 °C for 12 hours, then placed in a furnace at 500 °C for 90 min under nitrogen gas until activated. After that, hydrochloric acid 0.1 M was added to the activated carbon and boiled on the heater for 20 min, then removed from the heater and the activated carbon was separated and rinsed several times with hydrochloric acid 0.1 M and then rinsed repeatedly with distilled water to remove Cl^- ions from the activated carbon and neutralize the pH. The product was finally placed in the oven at 120 °C for 12 hours to dry [30]. Fig. 1 shows the changes from date fibers to activated carbon.

3. Magnetic Activated Carbon

First, 0.92 g of $FeCl_3{\cdot}6H_2O$ and 0.7 g of $FeSO_4{\cdot}7H_2O$ was dissolved in distilled water separately and the prepared solutions were placed under nitrogen gas. The above solutions were added to a flat bottom balloon and mixed together for 30 min on a mechanical stirrer (MIXT250M, Sanat Ceram, Iran). After that, 1 g of the synthesized activated carbon was added to distilled water and placed

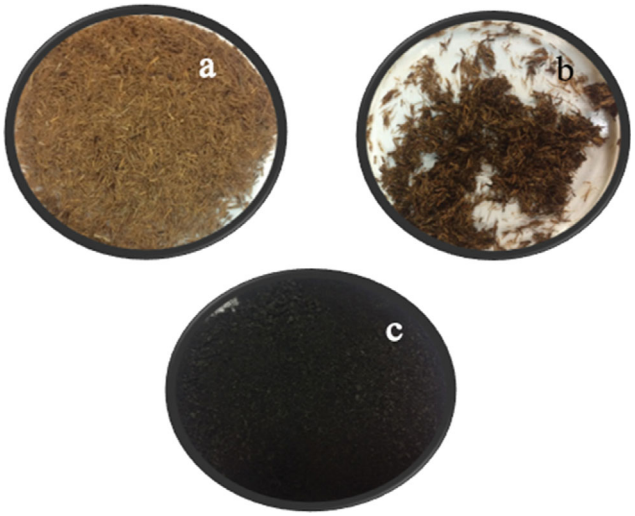

Fig. 1. Changes in date palm fiber during the production of activated carbon, (a) Palm fiber, (b) Phosphoric acid and palm fiber, and (c) Activated carbon (AC).

under sonication (TI-H-5, Elma, Germany), then added to the above solution and stirred for 30 min. After this step, about 10 mL of 10 M NaOH was added dropwise to the above solution to bring the pH above 10. After that, it was left for an hour to cool down and reach ambient temperature. At this stage, the magnetic-activated carbon particles were separated by a magnet and rinsed frequently with distilled water to bring the pH close to neutral. Finally, the particles were dried in an oven at 50 °C overnight [31].

4. Catalyst Specifications

To study the functional groups of particles Fourier transform infrared spectroscopy (FTIR, AVATAR, USA) was applied. The size and morphology of particles using a field emission scanning electron microscope (FE-SEM, MIRA III, TESCAN) were determined. The specific particle surface area was ascertained by BET analysis (BET, BELSORP MINI II, Japan), and the chemical composition of the particles by X-ray diffraction analysis (XRD, PW1730, PHILPS, Netherlands) was determined. Energy-dispersive X-ray spectroscopy (EDS, MIRA III SAMAX detector, TESCAN, Czech Republic) was applied for elemental analysis of the catalyst and the magnetic properties of particles were analyzed by a vibrating sample magnetometer (VSM, LBKFB, Meghnatis Daghigh Kavir Co, Iran).

5. Heterogeneous Fenton Experiments

The stock solution was prepared from direct dye at a concentration of 1,000 mg/L by mixing the dye powder with distilled water, and from this solution, the required concentrations were prepared.

To start each experiment, 100 mL of a sample with a specified concentration of DR80 was poured into a 250 cc Erlenmeyer flask and the catalyst dose was carefully weighed by a digital scale (HR200, A&D, Japan) and added to the sample. To adjust the pH, 0.1 M NaOH solution and 0.1 M H_2SO_4 solution were used and the pH was measured by a pH meter (L2012, Labtoron, Iran). Then a specific amount of persulfate (PS) was added to the solution. The samples were mixed on an incubator shaker (INNOVA 40, Eppendorf, Germany), and at the specified time, 10 mL of the sample was taken and ethanol was added to stop the reaction, then the catalyst with the magnet was removed from the solution and the DR80 residue was read by spectrophotometer (DR6000, HACH, USA) at 528 nm. Under optimal conditions, COD removal efficiency was also measured. From the initial concentration and residual concentration of dye and COD in each step, the percentage of dye and COD removal in that experiment was calculated by Eq. (1).

$$\%R = \left(\frac{C_0 - C}{C_0}\right) \times 100 \quad (1)$$

In this equation, C_0 represents the initial concentration of DR80 dye or COD, and C represents the final concentration of dye or COD at any time, %R is the percentage of removal.

6. Experimental Design

Box-Behnken design under response surface methodology (RSM) was used to determine the number of experiments and to consider the effect of combining independent variables on the dependent variable and data analysis. Experiments based on the range of each variable including pH (3, 5.5, and 8), catalyst dose (0.2, 0.6, and 1 g/L), activator dose (1, 5.5, and 10 mM) and contact time (2, 46, and 90 min) was identified. Variables ranges were selected based on literature review and expert knowledge relevant to the heterogeneous Fenton process and used for the dye removal. After the optimal conditions were determined, the effect of temperature (at 20, 30, 40, and 50 °C) and dye concentration (10, 25, 50, and 100 mg/L) on dye removal efficiency under optimal conditions were investigated.

RESULTS AND DISCUSSION

1. Characterization of the Catalyst

Fourier transform infrared (FTIR) spectroscopy (Fig. 2) in the spectral range of 400 to 4,000 cm^{-1} was utilized to identify the bonds and determine the functional groups at the catalyst. According to Table 4, the peaks of 2,922.68 cm^{-1} and 2,854.59 cm^{-1} are related to the C-H bond and the peak at 1,586.22 cm^{-1} was ascertained to be the C=O bond. The peak at 3,440.17 cm^{-1} is related to the O-H bond. Peaks of 2,922.68 cm^{-1} and 2,854.59 cm^{-1} indicate the presence of C-H functional groups on the surface of the AC/Fe_3O_4 catalyst. Peak 1,078.93 cm^{-1} belongs to the C-O group [31]. The peak of 581.42 cm^{-1} is attributed to the Fe-O bond, which confirms the presence of Fe_3O_4 in the structure of the catalyst [31,32].

The image and size of the magnetic particles were examined by field emission scanning electron microscopy (FE-SEM). As can be seen in Fig. 3, the Fe_3O_4 nanoparticles on the surface of AC have a

Table 4. Functional groups of AC/Fe_3O_4

Functional groups	Literature [33]	Wavenumber (cm^{-1})
O-H Stretching	3,300-3,600	3,440.17
C-H Stretching	2,850-2,970	2,854.59-2,922.68
C=O	1,540-1,800	1,586.22
O-H Bending	1,500-1,600	1,586.22
C-O	1,050-1,330	1,078.93
Fe-O	500-610	581.42

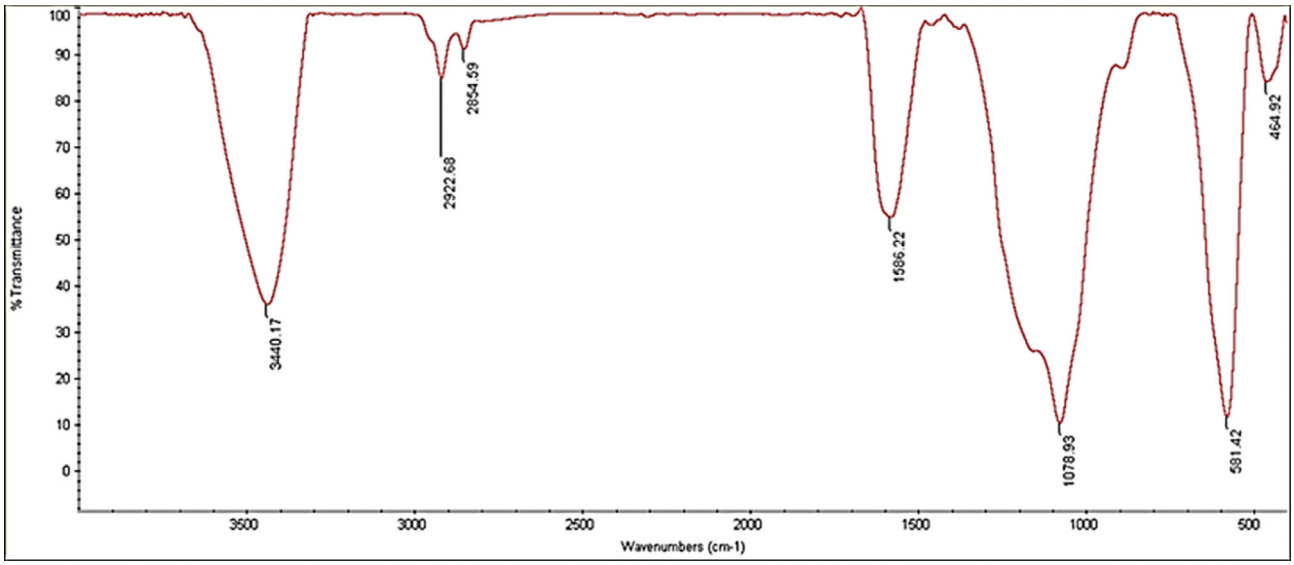

Fig. 2. FTIR spectrum of AC/Fe_3O_4 catalyst.

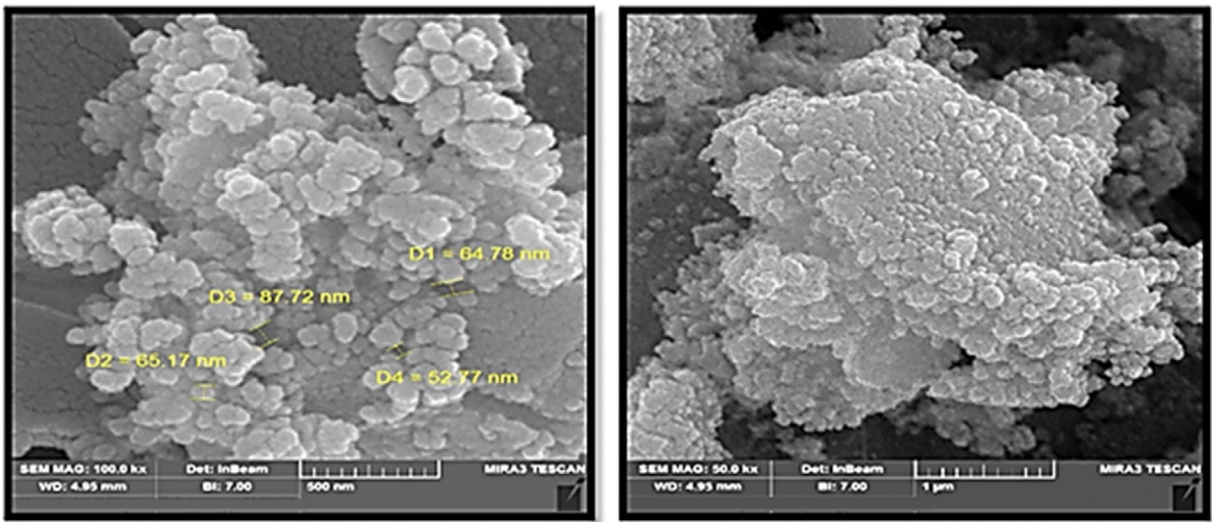

Fig. 3. FE-SEM images of AC/Fe_3O_4.

spherical shape and size in the range of 52-87 nm. The morphology of the AC surface is a solid that is heterogeneous but dominated by small particles that tend to be spherical [33].

The magnetic properties of AC/Fe_3O_4 magnetic activated carbon particles were evaluated by a vibrating sample magnetometer (VSM), and the results were plotted as a function of the magnetic field. As shown in Fig. 4, AC/Fe_3O_4 particles have a magnetic saturation level of about 17 emu/g. According to the results, AC/Fe_3O_4 particles have very good magnetic properties and can be easily separated by an external magnetic field, which indicates that AC/Fe_3O_4 has a high magnetic sensitivity. Overall, it is clear that AC/Fe_3O_4 can be easily and quickly separated from the solution and as a recyclable magnetic catalyst [32] used in aqueous solutions to remove contaminants.

To identify the crystal structure of the catalyst, X-ray diffraction (XRD) spectroscopy was performed at an angle of 2θ=10-80. The highest peaks (Fig. 5) in XRD analysis at 2θ=30.31, 35.81, 43.46, 54.26, 57.31, and 62.96 degrees, confirm the presence of Fe_3O_4 nanoparticles in AC/Fe_3O_4 [32]. Also, a peak at the angle of 28.06 degree, indicates that the carbon is amorphous [33].

Specific surface area, volume and average pore diameter on AC/Fe_3O_4 were measured by BET analysis, and the results (Table 5) showed that the specific surface area of magnetic particles was 1,220.8 m^2/g. The pore volume at relative pressure (P/P_0) 0.990 was 0.8064 cm^3/g. According to the IUPAC classification, (micropore (d<2 nm), mesopore (2<d<50 nm) and macropore (d>50 nm), the average pore size of catalyst in BET analysis is equal to 2.642 nm

Table 5. BET and structural specifications of AC/Fe_3O_4

$a_{s,BET}$	1,220.8	(m^2/g)
Total pore volume (P/P_0=0.990)	0.8064	(cm^3/g)
Mean pore diameter	2.6422	(nm)

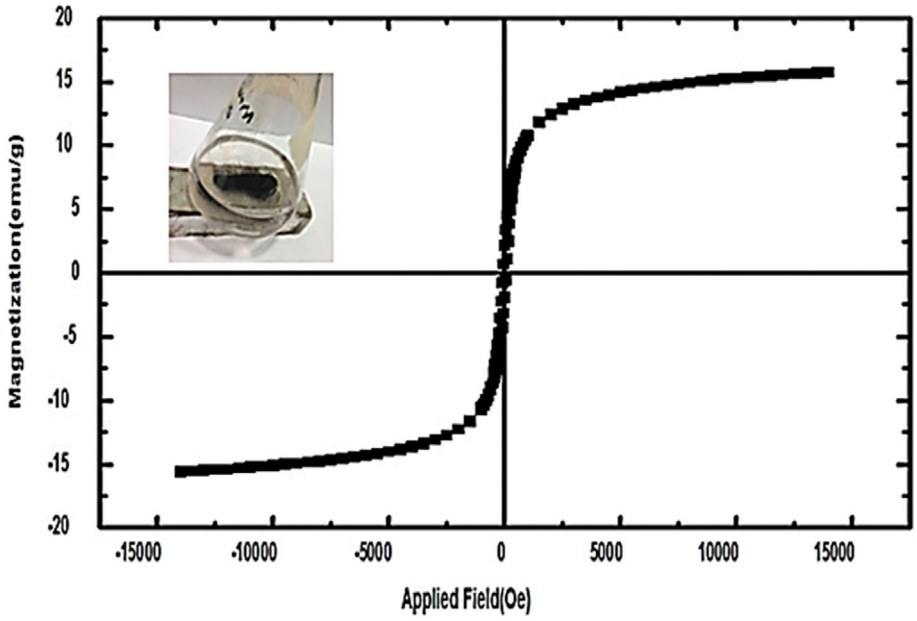

Fig. 4. VSM diagram of AC/Fe_3O_4 particles.

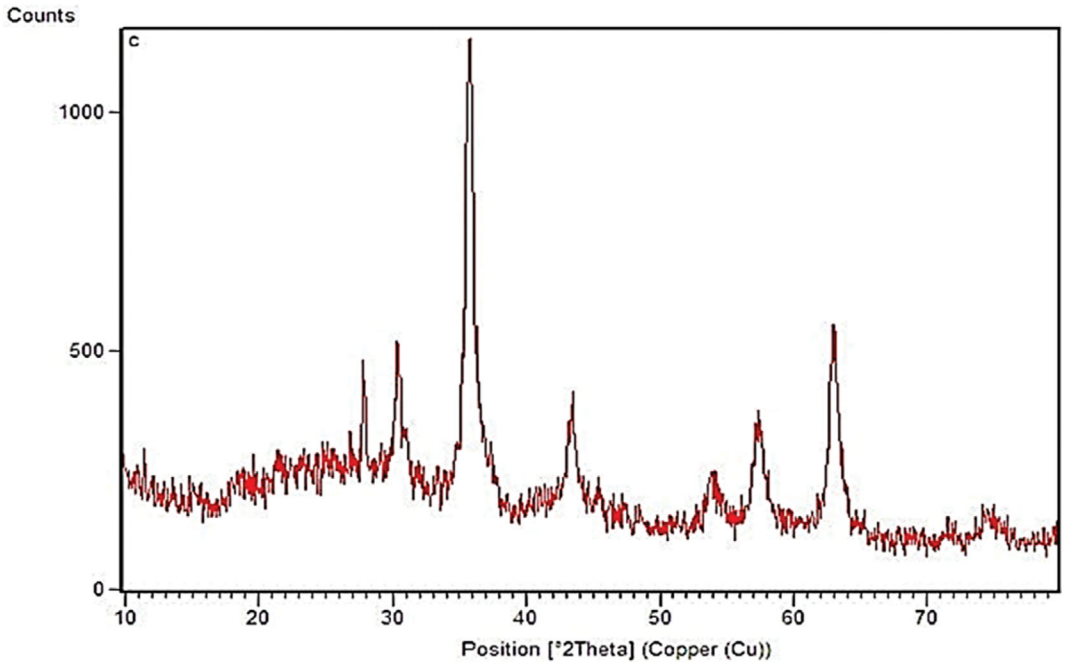

Fig. 5. XRD pattern for AC/Fe_3O_4.

and in the range of mesopores [34,35]. The pore size of magnetic activated carbon produced from palm kernel shell has been reported 3.39 nm, which is in the range of mesopore size [36].

EDS analysis was used to determine the elements in the synthesized catalyst structure. The results of the AC/Fe_3O_4 catalyst analysis indicate (Fig. 6) the presence of elements such as iron and oxygen, both of which are the main elements of the process of magnetization of activated carbon [32,37]. Also, the weight percentage of elements in the catalyst structure showed that the amount of carbon, oxygen and iron was 26.17, 28.76 and 45.07%, respectively, and the elements were well dispersed according to the EDS maps (Fig. 7). Similar findings have been observed for magnetic activated carbon prepared from chestnut shell waste [38].

Jafari et al. studied removing tetracycline by the AC/Fe_3O_4/PS system in the Fenton-like process; they used VSM analysis to find the magnetic properties of AC/Fe_3O_4. The results showed that the magnetic saturation level in AC/Fe_3O_4 was around 6.6 emu/g. However, observations showed that the magnetic response was good when the catalyst was placed near the magnet. XRD analysis was performed in the range of 10-70°. The results for Fe_3O_4 showed sharp

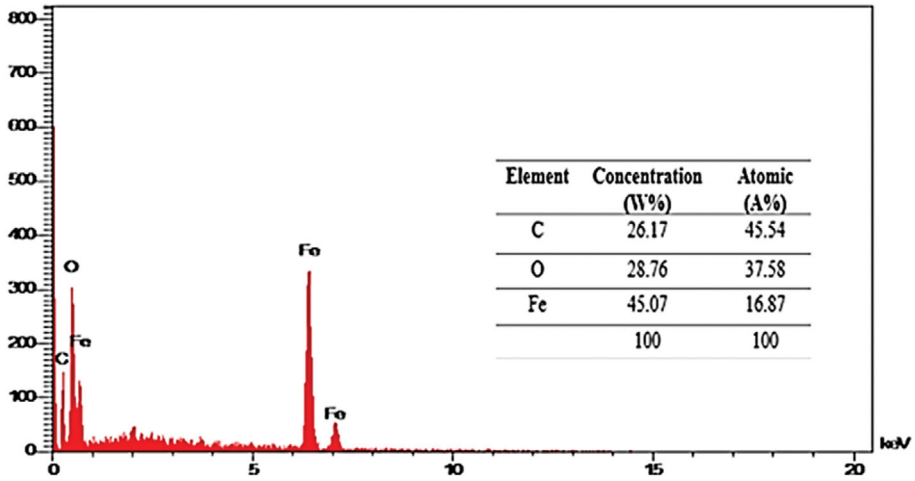

Fig. 6. EDS spectrum and components of AC/Fe_3O_4.

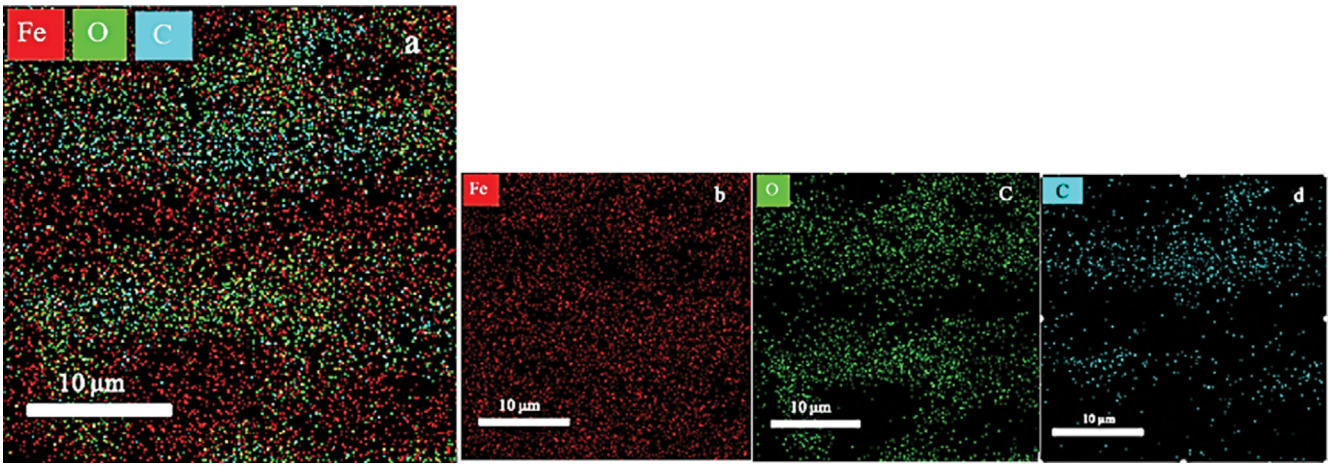

Fig. 7. EDS mapping: (a) Catalyst surface, (b) Iron, (c) Oxygen, and (d) Carbon.

peaks with 2θ values of 30.07 (220), 35.44 (311), 43.15 (400), 54.6 (422), 56.99 (511) and 62.6 (440) degrees in accordance with the standard (JCPDS No 19-0629) the cubic structure of Fe_3O_4 nanoparticles was confirmed [37].

2. Box-Behnken Design

Based on the Box-Behnken design, 29 experiments were performed to assess DR80 dye removal by heterogeneous Fenton process using magnetically activated carbon catalyst, and the results are presented in Table 6.

3. Statistical Analysis

The analysis of variance results are presented in Table 7. The P-value less than 0.0001 and the Lack of fit above 0.05 [39] and the high F-value of 58.67 indicate the model is statistically acceptable [40,41]. Also, the value of R^2 (R-Squared) is high and close to one. According to Table 7, the regression coefficient R^2 of the model was 0.951, which is an acceptable result [42]. In the table, codes A, B, C, and D represent the independent variables of pH, catalyst dose, activator dose, and contact time, respectively.

The data obtained from the experiments were analyzed and the dye removal efficiency in different conditions was estimated by a second-order polynomial model according to Eq. (2):

$$\text{Removal (\%)} = +53.12 + 1.57*A + 16.80*B + 12.45*C + 16.52*D + 4.02*A*C + 4.77*B*C - 3.94*B*D - 3.95*C^2 \quad (2)$$

In this equation, the effect of each variable is denoted by a positive sign (+) or a negative sign (−). A, B, C, and D represent the coded value of independent variables, such as pH, catalyst dose, activator dose, and contact time, respectively. According to the results, all studied independent variables have a positive effect on dye removal. Based on the results, the optimum conditions to reach the highest dye removal efficiency were catalyst dose 0.96 g/L, activator dose 9.7 mM, pH 7 and contact time 84 min. At this condition, maximum dye removal was 92.69%, which was very close to the predicted value of 93% by the model. To show the power of the heterogeneous Fenton process (activator+catalyst) for dye removal, at the optimum condition, the dye removal efficiency was evaluated in two states: the absence of the catalyst and another in the absence of the activator. In the absence of the catalyst and activator, the dye removal efficiency was 7.93 and 13.22%, respectively. These results indicate the catalyst in the presence of activator during the heterogeneous Fenton process can remarkably remove direct dye as high as 92.69%.

Table 6. Results for DR80 removal

Run	pH	Catalyst (g/L)	Activator (mmol)	Time (min)	Dye removal (%)
1	5.5	1	10	46	84.64
2	8	1	5.5	46	70.81
3	5.5	0.6	5.5	46	49.54
4	5.5	1	5.5	90	78.21
5	3	1	5.5	46	65.58
6	5.5	1	1	46	55.06
7	5.5	0.6	5.5	46	51.33
8	5.5	0.6	5.5	46	50.25
9	5.5	0.2	10	46	36.53
10	5.5	0.6	10	90	78.36
11	3	0.6	1	46	36.95
12	3	0.2	5.5	46	28.85
13	3	0.6	10	46	55.47
14	5.5	1	5.5	2	55.37
15	8	0.6	10	46	70.12
16	5.5	0.2	5.5	90	59.60
17	8	0.6	5.5	90	72.47
18	8	0.2	5.5	46	36.03
19	5.5	0.2	5.5	2	21.02
20	5.5	0.6	5.5	46	58.71
21	5.5	0.2	1	46	26.02
22	8	0.6	5.5	2	36.70
23	5.5	0.6	1	90	47.12
24	3	0.6	5.5	2	38.04
25	5.5	0.6	10	2	44.62
26	3	0.6	5.5	90	77.93
27	8	0.6	1	46	35.54
28	5.5	0.6	1	2	19.66
29	5.5	0.6	5.5	46	52.64

Fig. 8 was drawn to determine the accuracy of the model. According to Fig. 8(a), the observed values and the predicted values (by the model) of direct red 80 dye removal have a high correlation. Fig. 8(b) shows the distribution of residuals. The data distribution is normal and the data is well distributed around a straight line. Fig. 8(c) shows the random distribution of the residuals in the range of −3 and 3, which shows the good quality of the model in predicting removal efficiency.

4. Influence of Heterogeneous Fenton Process Parameters on Dye Removal Efficiency

Three-dimensional diagrams show the interaction effect of independent parameters on dye removal at the heterogeneous Fenton process. Fig. 9((a) to (f)) shows the interaction of pH and catalyst dose, pH and activator dose, pH and contact time, catalyst dose and activator dose, catalyst dose and contact time, and activator dose and contact time, respectively.

5. Effect of pH on Removal Efficiency

This study investigated the removal efficiency of DR80 by persulfate-based heterogeneous Fenton process at different pHs in the range of 3 to 8. In contrast to homogeneous Fenton, whose performance is limited to low-range pH, persulfate-based heterogeneous Fenton showed good efficiency in a wide range of pH and the results revealed that pH variation had a slight effect on DR80 removal efficiency. Zhang et al. used the heterogeneous Fenton process to degrade tetrabromo bisphenol A by Fe_3O_4@β-CD/MWCNT nanocomposite. The results show that the degradation efficiency of bisphenol A increases with decreasing pH [22]. In Zhang et al's study, they applied the heterogeneous Fenton process to remove fluconazole with Cu-V bimetallic catalysts. The results showed that the degradation efficiency decreased with increasing pH. At pH 3 for 60 min, the contaminant was completely removed. However, at pH 5, 7, and 9 the fluconazole oxidation efficiency remained above 90% and the wide pH adaptation to the $CuVOx/H_2O_2$ system may be attributed to vanadium due to the formation of multiple active centers on the catalyst surface [43]. Note that in this study, potassium persulfate was used to activate the heterogeneous Fenton process, which may be an influential factor in the pH of the neutral range.

6. Effect of Catalyst Dose on Removal Efficiency

The effect of AC/Fe_3O_4 catalyst dose on DR80 removal effi-

Table 7. ANOVA results for dye removal efficiency

Source	Sum of squares	Degree of freedom	Mean square	F-value	p-Value	Status
Model	8,879.65	8	1,109.96	58.67	<0.0001	Significant
A	29.67	1	29.67	1.57	0.2249	
B	3,387.55	1	3,387.55	179.05	<0.0001	
C	1,859.78	1	1,859.78	98.30	<0.0001	
D	3,275.59	1	3,275.59	173.13	<0.0001	
AC	64.48	1	64.48	3.41	0.0797	
BC	90.92	1	90.92	4.81	0.0404	
BD	61.94	1	61.94	3.27	0.0855	
C^2	109.72	1	109.72	5.80	0.0258	
Residual	378.40	20	18.19			
Lack of fit	324.62	16	20.29	1.51	0.3731	Not significant
Cor total	9,258.04	28				

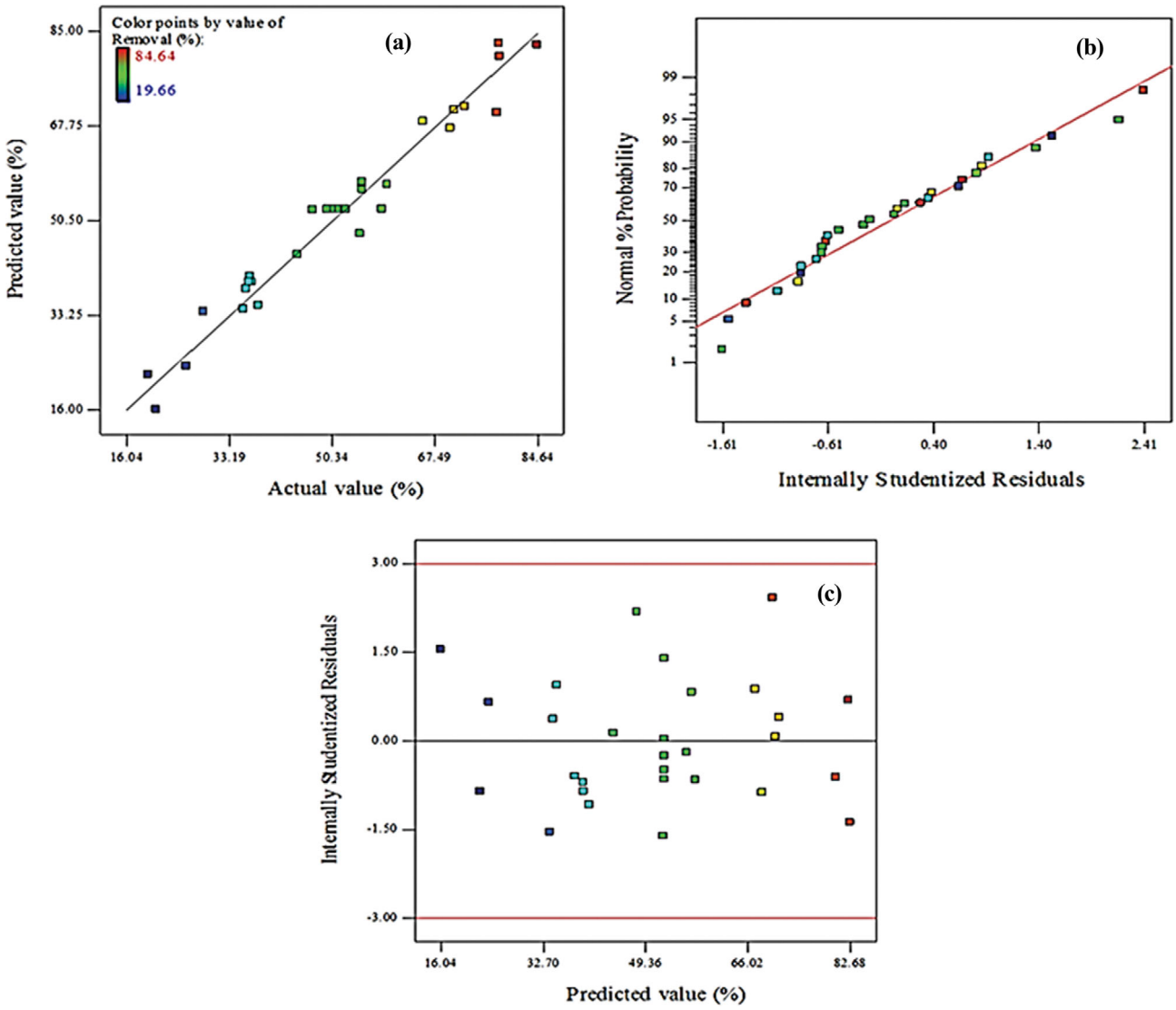

Fig. 8. Actual DR80 removal values versus predicted values (a), Normal probability (b), and Random distribution (c).

ciency was investigated and based on ANOVA results, AC/Fe_3O_4 catalyst dose is the most effective parameter on dye removal. The dye removal efficiency increases with increasing catalyst dose from 0.2 to 1 g/L. Zhang et al. used the heterogeneous Fenton process to degrade tetrabromobisphenol A by Fe_3O_4@β-CD/MWCNT nanocomposite. The results showed that by increasing the catalyst dose from 0.2 to 0.5 g/L, the degradation efficiency of TBBPA improved from 44.1 to 89.7% [44]. Yang et al., on the degradation of 4-chlorophenol (4-CP) with Zn_0-CNTs-Fe_3O_4 catalyst in the heterogeneous Fenton process, showed that increasing the dose of Zn_0-CNTs-Fe_3O_4 from 0.5 to 2 g/L efficiency enhanced and the highest removal efficiency of 99% was observed after 20 min with a catalyst dose of 2 g/L [20].

7. Effect of PS Dose on Removal Efficiency

The effect of PS dose on DR80 dye removal efficiency was investigated and the results showed that DR80 removal efficiency increased with increasing PS dose from 1 to 10 mM. Persulfate is a source of sulfate radicals and more sulfate radicals are produced at higher doses of persulfate according to Eqs. (3) and (4).

$$S_2O_8^{2-} + Fe^{2+} \rightarrow SO_4^{\bullet-} + SO_4^{2-} + Fe^{3+} \quad (3)$$

$$SO_4^{\bullet-} + Fe^{2+} \rightarrow SO_4^{2-} + Fe^{3+} \quad (4)$$

In the study of Lie et al., the decolorization efficiency of AO7 in the Fe^{3+}/H_2A/PS system increased from 67.8 to 92.5% by increasing the concentration of persulfate from 2 to 2.5 mM [45]. These results are consistent with the results presented in other articles [46, 47]. The rise in sulfate radical activity compared to hydroxyl radicals is due to its longer lifespan; this increase in lifespan increases the effective collision between pollutant molecules and sulfate radicals compared to hydroxyl radicals [48].

8. Effect of Contact Time on Dye Removal Efficiency

The contact time varied between 2-90 min and the DR80 removal efficiency was enhanced with increasing contact time. Also, the decolorization efficiency was measured under optimal conditions during different contact times to study the kinetic of the reaction.

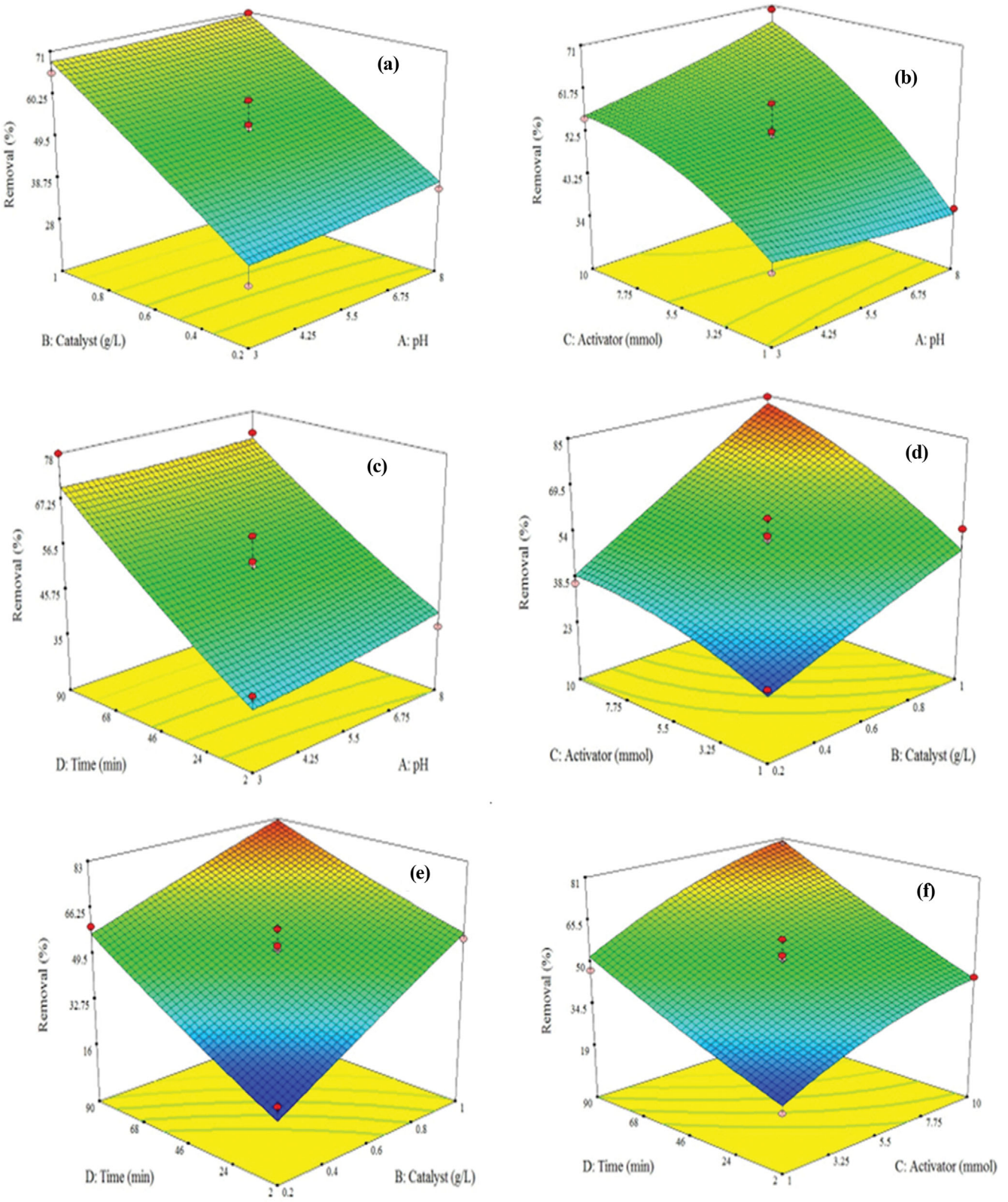

Fig. 9. Interaction of (a) Catalyst dose and solution pH, (b) Activator dose and solution pH, (c) Reaction time and solution pH, (d) Catalyst dose and activator dose, (e) Catalyst dose and reaction time, (f) Activator dose and reaction time.

The results showed that by increasing the contact time, the decolorization efficiency improved from 37.1 to 92.69%. This is because the sulfate radicals are longer in contact with the contaminant, and the efficiency enhances [46,47]. Also, the results followed pseudo-

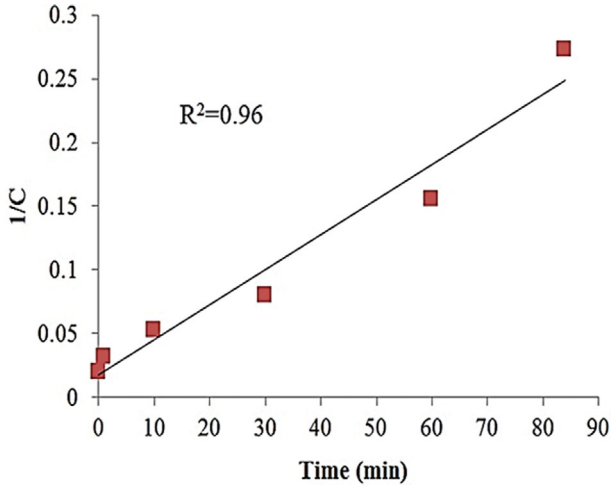

Fig. 10. Second-order kinetic plot in the optimal condition of the heterogeneous Fenton process.

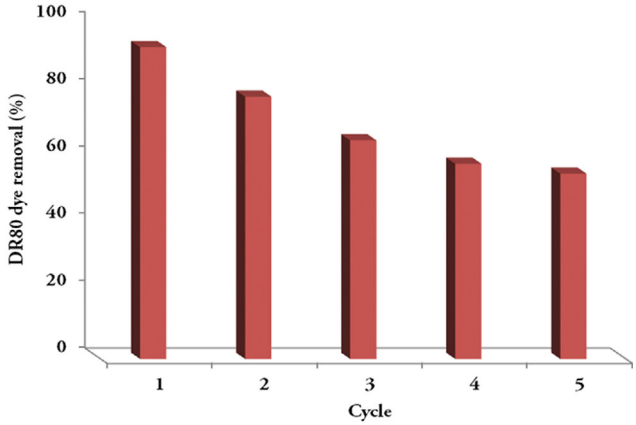

Fig. 11. Reuse of AC/Fe_3O_4 magnetic activated carbon catalyst for dye removal (catalyst dose 0.96 g/L, activator dose 9.7 mM, pH 7, and contact time 84 min).

second-order kinetic (R^2 0.96) according to Fig. 10 and the kinetic rate constant was 0.0027.

9. Effect of Temperature on Dye Removal Efficiency

Under optimal conditions, the effect of temperatures of 20, 30, 40 and 50 °C was investigated on dye removal. According to Table 8, with raising temperature from 20 to 50 °C, the efficiency increased from 87 to 98%, but with increasing temperature from 40 °C to 50 °C, no significant change was observed. The lifespan of persulfate and consequently sulfate radicals is relatively short at high temperatures [49]. Also, the effect of temperature on dye removal in the heterogeneous Fenton process can be explained by the two main processes involved: oxidation and coagulation. High temperature increases the kinetic energy and collision frequency of particles, which favors the rate of oxidation [50]. In the study of Kartal et al. in the temperature range of 45-60 °C with 2 mM $Na_2S_2O_8$ and the RR239 dye concentration of 40 mg/L, the degradation efficiency increased with raising of temperature up to 55 °C and no increase in efficiency was observed at higher temperatures [51].

10. Effect of Dye Concentration on the Removal Efficiency

At optimal conditions, by increasing the dye concentration from 10 to 25 mg/L, the efficiency was enhanced from 93 to 96%. However, by increasing the dye concentration from 25 to 100 mg/L, the process efficiency decreased from 96 to 69%. The rise in removal efficiency with increasing the initial dye concentration from 10 to 25 mg/L is mainly due to the increased effective collision between free radicals and dye molecules [52]. In a study by Hadi et al. for the removal of MB by heterogeneous Fenton-like process with persulfate activator, the results showed that with increasing MB concentration, the degradation efficiency decreased. High MB concentrations are likely to play an inhibitory role and reduce the amount of $SO_4^{\bullet-}$ radicals [47]. In AOPs, as the dye concentration increases, the various intermediates formed by the degradation of the primary dye may interfere with the desired oxidation. Such an event will be more obvious in the presence of a high level of degradation mediators caused by increasing dye concentration [53].

11. Reusability of AC/Fe_3O_4 Catalyst

In this study, the regeneration process was conducted in five cycles and the DR80 removal efficiency in each cycle was measured and presented in Fig. 11. According to the findings, DR80 dye removal efficiency in the heterogeneous Fenton process decreased from 92.69 to 55% after 5 cycles. These results indicate that AC/Fe_3O_4 can be used for several consecutive cycles with recyclability, as well as the ability to reuse the catalyst reduces the operating costs of wastewater treatment plants. However, the decrease in DR80 removal efficiency can be attributed to the mass loss of AC/Fe_3O_4 during the regeneration process. In addition, the reduction in removal efficiency in the regeneration process could be due to the loss of catalytic active sites in the washing stages of the catalyst. The DR80 removal efficiency after several regeneration cycles of the AC/Fe_3O_4 catalyst is shown in Fig. 11.

Khodadadi et al. investigated the reusability of $FeNi_3@SiO_2/H_2O_2$ catalyst in the heterogeneous Fenton process by measuring the removal efficiency of tetracycline (TC) in five cycles. Due to the loss of catalyst mass during washing and regeneration, the TC degradation efficiency decreased from 87 to 77% [54]. In a study by

Table 8. Effect of temperature under optimal conditions on dye removal efficiency (catalyst dose 0.96 g/L, activator dose 9.7 mM, pH 7, and contact time 84 min)

Run	Temperature (°C)	pH	Catalyst (g/L)	Activator (mM)	Contact time (min)	Dye removal efficiency (%)
1	20	7	0.96	9.7	84	87.07
2	30	7	0.96	9.7	84	92.74
3	40	7	0.96	9.7	84	98.63
4	50	7	0.96	9.7	84	98.71

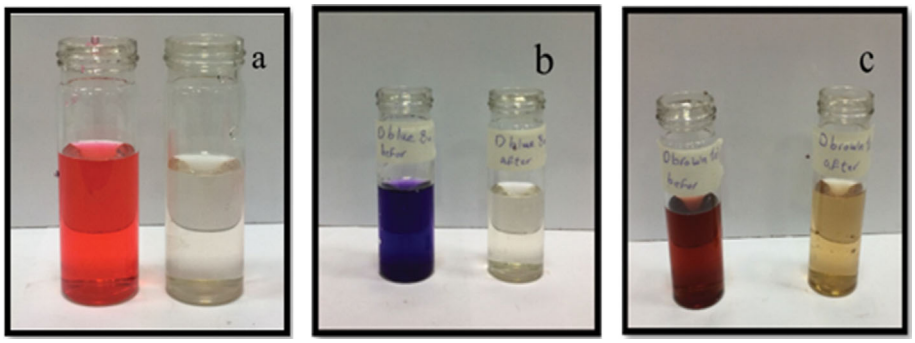

Fig. 12. Effect of heterogeneous Fenton process under optimal conditions on direct dyes removal (catalyst dose 0.96 g/L, activator dose 9.7 mM, pH 7, and contact time 84 min): (a) DR80, (b) DB80, and (c) DB103.

Table 9. Efficiency of various catalysts used for dye removal

Catalyst	Dye	Dye removal efficiency (%)	Reference
$MnFe_2O_4$-GO	Rhodamine B	97	[55]
Vermiculite	Ponceau SS	92.4	[56]
Fe_3O_4 nanoparticles	Methyl orange	86.6	[57]
Fe_3O_4/rGO	Reactive red 195	93.3	[58]
AC/Fe_3O_4/PS	Direct blue 80	97.07	This study

Kakavandi et al. to remove tetracycline from the AC/Fe_3O_4/PS system in a Fenton-like process, catalyst reuse was performed in five cycles and the efficiency decreased from 99.8 to 93.2% [37].

12. Removal of Different Direct Dyes

This study demonstrates the effective removal efficiency of DR80 using the AC/Fe_3O_4/PS system. To generalize the results of this study, the effect of the heterogeneous Fenton process under optimal conditions on direct blue 80 and direct brown 103 dye removal was investigated. The removal efficiency of direct blue 80 and direct brown 103 under optimal conditions (catalyst dose 0.96 g/L, activator dose 9.7 mM, pH 7 and contact time 84 min) was 97.07 and 73.85%, respectively, and the results show that the heterogeneous Fenton process with AC/Fe_3O_4/PS system has good performance in removing other direct dyes (Fig. 12). The difference in dye degradation behavior is probably attributed to the different molecular structures of the dyes.

The results from this study were compared with the efficiency of different catalysts in the removal of various dyes using heterogeneous Fenton process, and the data given in Table 9. From this table, it is clear that the AC/Fe_3O_4 catalyst has significantly reduced the DR80 dye.

CONCLUSION

AC/Fe_3O_4 catalyst was successfully synthesized through a simple method. The heterogeneous Fenton process with magnetic activated carbon produced from date palm waste in the presence of persulfate has a high potential to remove direct dyes from aqueous solution. 92.69, 97.07, and 73.85% of Direct Red 80, Direct Blue 80, and Direct Brown 103 were removed at optimal conditions of catalyst dose 0.96 g/L, activator dose 9.7 mM, pH 7, and contact time 84 min. Analysis of variance (ANOVA) showed the accuracy of the proposed model for the degradation of DR80 dye by the heterogeneous Fenton process (R^2 0.951). AC/Fe_3O_4 as a reusable catalyst not only has a good ability to remove pollutants but also is also environmentally friendly. After five cycles of catalyst regeneration, the results demonstrated the high ability of the catalyst for dye removal. It also has good properties such as high surface area, and good magnetic properties which led to improved performance.

ACKNOWLEDGEMENT

The authors thank the support of Shahid Sadoughi University of Medical Sciences (Grant No: 7565).

REFERENCES

1. M. Hasanzadeh, A. Simchi and H. S. Far, *J. Ind. Eng. Chem.*, **81**, 405 (2020).
2. A. C. Lucilha, C. E. Bonancêa, W. J. Barreto and K. Takashima, *Spectroc. Acta Pt. A-Molec. Biomolec. Spectr.*, **75**, 389 (2010).
3. T. C. Egbosiuba, A. S. Abdulkareem, A. S. Kovo, E. A. Afolabi, J. O. Tijani, M. Auta and W. D. Roos, *Chem. Eng. Res. Des.*, **153**, 315 (2020).
4. F. Kallel, F. Bouaziz, F. Chaari, L. Belghith, R. Ghorbel and S. E. Chaabouni, *Process Saf. Environ. Protect.*, **102**, 30 (2016).
5. J. d. J. da Silveira Neta, G. C. Moreira, C. J. da Silva, C. Reis and E. L. Reis, *Desalination*, **281**, 55 (2011).
6. S. M. Pormazar and A. Dalvand, *Korean J. Chem. Eng.*, **37**, 2192 (2020).
7. Z. Cheng, L. Zhang, X. Guo, X. Jiang and T. Li, *Spectroc. Acta Pt. A-Molec. Biomolec. Spectr.*, **137**, 1126 (2015).
8. J. Alagesan, M. Jaisankar, S. Muthuramalingam, E. Mousset and

P. V. Chellam, *Chemosphere*, **262**, 128381 (2021).
9. S. Álvarez-Torrellas, G. Ovejero, R. García-Lovera, A. Rodríguez and J. García, *Clean Technol. Environ. Policy*, **18**, 1085 (2016).
10. M. Nawaz, W. Miran, J. Jang and D. S. Lee, *Catal. Today*, **282**, 38 (2017).
11. Y. A. Patil, B. Sadhu, D. R. Boraste, A. L. Borkar and G. S. Shankarling, *J. Mol. Struct.*, **1202**, 127278 (2020).
12. S. Saber-Samandari, S. Saber-Samandari, H. Joneidi-Yekta and M. Mohseni, *Chem. Eng. J.*, **308**, 1133 (2017).
13. E. H. C. de Oliveira, D. M. d. S. M. Fraga, M. P. da Silva, T. J. M. Fraga, M. N. Carvalho, E. M. P. de Luna Freire, M. G. Ghislandi and M. A. da Motta Sobrinho, *J. Environ. Chem. Eng.*, **7**, 103001 (2019).
14. A. Abd-Elhamid, E. A. Kamoun, A. A. El-Shanshory, H. M. Soliman and H. Aly, *J. Mol. Liq.*, **279**, 530 (2019).
15. U. Tyagi, *Groundwater Sust. Dev.*, **10**, 100303 (2020).
16. K. Rubeena, P. H. P. Reddy, A. Laiju and P. Nidheesh, *J. Environ. Manage.*, **226**, 320 (2018).
17. J. Du, S. H. Kim, M. A. Hassan, S. Irshad and J. Bao, *Environ. Sci. Pollut. Res.*, **27**, 37286 (2020).
18. S. Xiao, M. Cheng, H. Zhong, Z. Liu, Y. Liu, X. Yang and Q. Liang, *Chem. Eng. J.*, **384**, 123265 (2020).
19. M. O. Omorogie, A. E. Ofomaja, *Clean Technol. Environ. Policy*, **19**, 2191 (2017).
20. Z. Yang, X. B. Gong, L. Peng, D. Yang and Y. Liu, *Chemosphere*, **208**, 665 (2018).
21. S. J. Mazivila, I. A. Ricardo, J. M. Leitão and J. C. E. da Silva, *Trends Environ. Anal. Chem.*, **24**, e00072 (2019).
22. M. H. Zhang, H. Dong, L. Zhao, D. X. Wang and D. Meng, *Sci. Total Environ.*, **670**, 110 (2019).
23. Y. Zhu, R. Zhu, Y. Xi, J. Zhu, G. Zhu and H. He, *Appl. Catal. B: Environ.*, **255**, 117739 (2019).
24. O. L. Nwanji, M. O. Omorogie, J. O. Babalola and J. O. Olowoyo, *Biomass Conv. Biorefinery*, **11**, 1853 (2021).
25. P. Sreeja and K. Sosamony, *Procedia Technol.*, **24**, 217 (2016).
26. M. Jose, K. Sriram, R. Reshma, U. Vidya and S. Shukla, *J. Environ. Chem. Eng.*, **6**, 3709 (2018).
27. P. Nidheesh and R. Rajan, *RSC Adv.*, **6**, 5330 (2016).
28. M. Adeli Sardooei, M. Khodaverdizadeh and O. Esmaeilipour, *Int. J. Agric. Manage. Dev.*, **11**, 455 (2021).
29. B. D'Cruz, M. Madkour, M. O. Amin and E. Al-Hetlani, *Mater. Chem. Phys.*, **240**, 122109 (2020).
30. H. Zhang, Y. Yan and L. Yang, *Adsorpt. Sci. Technol.*, **26**, 533 (2008).
31. M. Hosseinzehi, M. H. Ehrampoush, F. Tamaddon, M. Mokhtari and A. Dalvand, *Int. J. Environ. Anal. Chem.*, 1 (2021).
32. X. Song, J. Mo, Y. Fang, S. Luo, J. Xu and X. Wang, *Environ. Sci. Pollut. Res.*, **29**, 35204 (2022).
33. D. Dirgayanti, S. Koesnarpadi and N. Hindryawati, *IOP conference series: Earth and environmental science*, IOP Publishing, 012070 (2021).
34. R. Rezaei Kalantry, A. Jonidi Jafari, A. Esrafili, B. Kakavandi, A. Gholizadeh and A. Azari, *Desalin. Water Treat.*, **57**, 6411 (2016).
35. A. Azari, H. Gharibi, B. Kakavandi, G. Ghanizadeh, A. Javid, A. H. Mahvi, K. Sharafi and T. Khosravia, *J. Chem. Technol. Biotechnol.*, **92**, 188 (2017).
36. C. Anyika, N. A. M. Asri, Z. A. Majid, A. Yahya and J. Jaafar, *Nanotechnol. Environ. Eng.*, **2**, 1 (2017).
37. A. J. Jafari, B. Kakavandi, N. Jaafarzadeh, R. R. Kalantary, M. Ahmadi and A. A. Babaei, *J. Ind. Eng. Chem.*, **45**, 323 (2017).
38. S. Rodríguez-Sánchez, B. Ruiz, D. Martínez-Blanco, M. Sánchez-Arenillas, M. A. Diez, J. F. Marco, P. Gorria and E. Fuente, *Appl. Surf. Sci.*, **551**, 149407 (2021).
39. A. Manassa and P. Seesuriyachan, *Biomass Conv. Biorefinery*, **11**, 1029 (2021).
40. H. Zarei, S. Nasseri, R. Nabizadeh, F. Shemirani, A. Dalvand and A. H. Mahvi, *Desalin. Water Treat.*, **67**, 196 (2017).
41. S. M. Pormazar and A. Dalvand, *Int. J. Environ. Anal. Chem.*, **102**, 1764 (2022).
42. W. Srimoke, V. Kanokkantapong, N. Supakata and W. Limmun, *Arabian J. Chem.*, **15**, 104213 (2022).
43. N. Zhang, C. Xue, K. Wang and Z. Fang, *Chem. Eng. J.*, **380**, 122516 (2020).
44. Y. Zhang, P. Wu, Z. Chen, L. Zhou, Y. Zhao, Y. Lai, Y. Duan, F. Wang and S. Li, *Mater. Res. Bull.*, **113**, 14 (2019).
45. Y. Lei, H. Zhang, J. Wang and J. Ai, *Chem. Eng. J.*, **270**, 73 (2015).
46. A. H. Hilles, S. S. A. Amr, R. A. Hussein, O. D. El-Sebaie and A. I. Arafa, *J. Environ. Manage.*, **166**, 493 (2016).
47. S. Hadi, E. Taheri, M. M. Amin, A. Fatehizadeh and R. L. Gardas, *J. Mol. Liq.*, **328**, 115408 (2021).
48. P. V. Nidheesh, *Environ. Sci. Pollut. Res.*, **24**, 27047 (2017).
49. R. L. Johnson, P. G. Tratnyek and R. O. B. Johnson, *Environ. Sci. Technol.*, **42**, 9350 (2008).
50. M. M. Arimi, *Prog. Nat. Sci.: Mater. Int.*, **27**, 275 (2017).
51. O. E. Kartal, *Am. J. Phys. Chem.*, **7**, 45 (2018).
52. K. Sarath, R. Gandhimathi, S. Ramesh and P. Nidheesh, *Desalin. Water Treat.*, **57**, 11872 (2016).
53. S. A. Kordkandi and M. Forouzesh, *J. Taiwan Inst. Chem. Eng.*, **45**, 2597 (2014).
54. M. Khodadadi, A. H. Panahi, T. J. Al-Musawi, M. Ehrampoush and A. Mahvi, *J. Water Process Eng.*, **32**, 100943 (2019).
55. G. Anil, J. Scaria and P. V. Nidheesh, *Water*, **14**, 3350 (2022).
56. A. J. Dos Santos, I. Sirés, A. P. Alves, C. A. Martínez-Huitle and E. Brillas, *Chemosphere*, **240**, 124838 (2020).
57. H. Jiang, Y. Sun, J. Feng and J. Wang, *Water Sci. Technol.*, **74**, 1116 (2016).
58. P. Nazari and S. Setayesh, *Int. J. Environ. Sci. Technol.*, **16**, 6329 (2019).